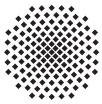

Universität Stuttgart

SimTech
Cluster of Excellence

M. Daub[a] · **S. Waldherr**[b] · **F. Allgöwer**[b] · **P. Scheurich**[c] · **G. Schneider**[a]

Death wins against life in a spatially extended model of the caspase-3/8 feedback loop

Stuttgart, Januar 2012

[a] Institute of Analysis, Dynamics and Modelling, University of Stuttgart,
Pfaffenwaldring 57, 70569 Stuttgart/ Germany
{Markus.Daub, Guido.Schneider}@mathematik.uni-stuttgart.de
www.iadm.uni-stuttgart.de/LstAnaMod/Schneider/

[b] Institute for Systems Theory and Automatic Control, University of Stuttgart,
Pfaffenwaldring 9, 70569 Stuttgart/ Germany
{Waldherr,allgower}@ist.uni-stuttgart.de
www.ist.uni-stuttgart.de

[c] Institute of Cell Biology and Immunology, University of Stuttgart,
Allmandring 31, 70569 Stuttgart/ Germany
Peter.Scheurich@izi.uni-stuttgart.de
www.uni-stuttgart.de/izi

Abstract Apoptosis is an important physiological process which enables organisms to remove unwanted or damaged cells. A mathematical model of the extrinsic pro-apoptotic signaling pathway has been introduced by Eissing et al [6] and a bistable behavior with a stable death state and a stable life state of the reaction system has been established.
In this paper, we consider a spatial extension of the extrinsic pro-apoptotic signaling pathway incorporating diffusion terms and make a model-based, numerical analysis of the apoptotic switch in the spatial dimension. For the parameter regimes under consideration it turns out that for this model diffusion homogenizes rapidly the concentrations which afterward are governed by the original reaction system. The activation of effector-caspase 3 depends on the space averaged initial concentration of pro-caspase 8 and pro-caspase 3 at the beginning of the process.

Preprint Series **Issue No. 2012-03**
Stuttgart Research Centre for Simulation Technology (SRC SimTech)
SimTech – Cluster of Excellence
Pfaffenwaldring 7a
70569 Stuttgart
publications@simtech.uni-stuttgart.de
www.simtech.uni-stuttgart.de

1 Introduction

Apoptosis is a common form of programmed cellular death and represents an important physiological process in multicellular organisms allowing the removal of unneeded, damaged or infected cells [4, 20]. Apoptosis can be induced by different stimuli to activate the extrinsic or the intrinsic pathway. The extrinsic pathway is initiated by activation of so-called death receptors, located in the plasma membrane, through binding of their respective death ligands [4, 8]. The intrinsic pathway is activated by cellular damage caused by e.g. ultraviolet irradiation at the DNA level or by toxic agents, which can lead to activation of the protein p53 and subsequent induction of apoptosis via the mitochondrion [8].

Both the extrinsic and the intrinsic pathways converge at the level of the caspase cascade, a network of specific proteases, the caspases, that is commonly recognized as the central and executing machinery of apoptosis [8, 19]. In apoptosis induction, two major types of caspases are distinguished: the initiator caspases, which get activated through cleavage for example in the death inducing signaling complex (DISC) of activated death receptors, and the effector caspases, which cleave multiple essential proteins thereby dismantling the cell [4, 19]. According to the current view, the point of no return is reached and the cell is irreversibly committed to die at a certain percentage of effector caspase activation. This percentage might be highly dependent of the particular cell type.

The relevance of the caspase cascade for apoptosis induction and execution has stimulated the development of mathematical models in order to better understand regulation of cell death. Early models formulated the activation of the caspase cascade via the extrinsic pathway [1, 5, 7]. Later models also considered the intrinsic pathway and its activation of the caspase cascade [17]. Especially through the analysis done in [5], using a minimized model of the cascade, it became apparent that bistability is a useful concept in order to combine fast caspase activation kinetics with tolerance towards a minute initiator caspase activation [13].

Bistability of the caspase cascade is essentially based on a positive feedback between initiator and effector caspases, in the sense that not only initiator caspases can cleave and activate effector caspases, but also vice versa. Properties of bistability of the caspase cascade and the underlying mechanisms were further analyzed in more simplistic models [6]. As one of their main conclusions, Eissing et al. find that model variants with cooperativity in caspase activation, binding of caspase 3 to an inhibitor, or zero-order ultrasensitivity in caspase degradation are similarly able to generate bistability, [6].

Recently, the spatial organization of caspase activation within cells has gained increased interest. While the switch-like behavior of effector caspase activation is well established for single cells in the dimension of time, this property is less clear in the spatial dimensions. In a first approach to investigate this issue, the organization of mitochondrial membrane permeabilization, a crucial initiating event in the intrinsic pathway of apoptosis, was studied [18]. In this study, the authors observed that mitochondrial membrane permeabilization occurs in a spatial wave within the cell. In a later study from the same group, it was additionally shown that caspase activation proceeds very quickly through the cell, apparently rendering the caspase substrate cleavage practically spatially homogeneous with respect to the relevant timescale [11]. These studies support the idea that caspase activation is also switch-like in the spatial dimension.

The goal of the present paper is to provide a model-based, numerical analysis of the apoptotic switch in the spatial dimension, considering a simplified spatial caspase activation model based on [6]. In [6] a mathematical model for the core of a simplified, protease-based activation cascade has been introduced, represented by e.g. the extrinsically triggered caspase cascade in a typical type I cell, where the concentration of (pro-) caspase 3 and (pro-) caspase 8 were modeled by a four-dimensional system of ordinary differential equations (ODE). This model is best reflected in biology by a highly sensitive type I cell, like KYM-1 [15].

The ODE system exhibits two asymptotically stable steady states. One represents the life state of the cell and is called $X^{(l)}$ in the following. The other is identified with the cellular death state and is called $X^{(d)}$. Because of the spatial extension of cells and because of the occurrence of the starting signal for the cell death at the cell membrane in the case of an extrinsic stimulus, it is of interest to consider a spatially extended version of the ODE model given in [6]. Since the model variants with cooperativity in caspase activation, binding of caspase 3 to an inhibitor, and zero-order ultrasensitivity were shown to behave similarly concerning bistability, we study only the first variant where bistability is generated by cooperativity. This explicitly excludes the well-known binding of caspase 3 to the inhibitor IAP,

but from the analysis in [6], cooperativity and inhibition are two equally useful mechanism to generate bistability.

The simplest way to obtain a spatially extended model is to incorporate diffusion of caspase molecules. This is done in Section 2. The steady states and their stabilities in the reaction-diffusion system are computed in Section 3. The initial value problem for a number of special concentration profiles is analyzed by numerical simulations. The results are presented in Section 4. It turns out that for the parameter regimes under consideration diffusion homogenizes rapidly the concentrations. After the homogenization they are governed by the original ODE model. For biologically relevant parameters the cell turns out to be too small for the exhibition of non trivial spatial structures in the apoptosis process. This is finally shown in A.

Acknowledgment. The authors would like to thank the German Research Foundation (DFG) for financial support of the project within the Cluster of Excellence in Simulation Technology (EXC 310/1) at the University of Stuttgart. This paper is partially supported by the "Center Systems Biology" (CSB) at the University of Stuttgart.

2 The reaction-diffusion model

In this section we recall the cooperative model proposed in [6] and introduce our extension of the model. In [6], the core of the pro-apoptotic extrinsic pathway is modeled by a four-dimensional ODE-system. This system describes the time evolution of (pro-) caspase 3 and (pro-) caspase 8 concentrations.
The reactions which are involved in the extrinsic pathway are the activation of pro-caspase 8 by caspase 3 and the activation of pro-caspase 3 by caspase 8

$$\mathrm{C8} + \mathrm{C3}^* \longrightarrow \mathrm{C8}^* + \mathrm{C3}^*, \qquad \mathrm{C3} + n\,\mathrm{C8}^* \longrightarrow \mathrm{C3}^* + n\,\mathrm{C8}^*, \tag{1}$$

where the star denotes the active form of the corresponding caspase and n describes cooperativity effects in the activation of caspase 3. Furthermore, pro-caspase 8 is activated by death receptors at the cell membrane. We introduce the concentrations

$$X_i = [\mathrm{C8}], Y_i = [\mathrm{C3}], X_a = [\mathrm{C8}^*], Y_a = [\mathrm{C3}^*] \tag{2}$$

of the four kinds of caspase. The concentrations are measured in the unit Molar.
Reaction rates are according to the law of mass action and it is assumed that pro-caspase 8 and pro-caspase 3 are produced in cells with a production rate k_{p1} and k_{p2}, respectively. Furthermore (pro-) caspase 8 and 3 is degraded in cells with degradation rates k_{d1}, k_{d2}, k_{d3} and k_{d4}, respectively. If we further take into account cooperativity effects described by the exponent n, then following [6] we obtain the system of ODEs

$$\begin{aligned} \dot{X}_a &= k_{c1} X_i Y_a - k_{d1} X_a, \\ \dot{Y}_a &= k_{c2} Y_i X_a^n - k_{d2} Y_a, \\ \dot{X}_i &= -k_{c1} X_i Y_a - k_{d3} X_i + k_{p1}, \\ \dot{Y}_i &= -k_{c2} X_a^n Y_i - k_{d4} Y_i + k_{p2}. \end{aligned} \tag{3}$$

We choose the parameter values

$$\begin{aligned} &k_{c1} = 8 \cdot 10^5\,\mathrm{M}^{-1}\mathrm{s}^{-1}, \qquad k_{c2} = 8 \cdot 10^{7n-2}\,\mathrm{M}^{-n}\mathrm{s}^{-1}, \\ &k_{p1} = k_{p2} = 1 \cdot 10^{-11}\,\mathrm{Ms}^{-1}, \; k_{di} = 0.03\,\mathrm{min}^{-1}, i = 1, \ldots, 4, \end{aligned} \tag{4}$$

close to the values in [5] and [6]. The exponent $n \geq 1$ for the cooperativity has no dimension and will be specified below. The reaction rate k_{c2} depends on the exponent n according to the units of the reaction system (3).

Since cells are spatially extended and since the starting signal for the extrinsic signaling pathway is given at the cell membrane it makes sense to consider a spatially extended version of the ODE model from [6]. The simplest way to do so is to incorporate diffusion of the caspases into the model. So, we introduce the spatial variable $x \in \mathbb{R}^d$ with d the space dimension, and extend (3) by adding the diffusion terms $(d_1 \Delta_x X_a, d_2 \Delta_x Y_a, d_3 \Delta_x X_i, d_4 \Delta_x Y_i)$, with diffusion coefficients $d_j, j = 1, \ldots, 4$,

similarly to other spatially extended models in mathematical biology, cf. for instance [16, Sec. 11.2]. The spatial domain under consideration is $\Omega = \{x \in \mathbb{R}^d, \|x\| \leq L\}$, i.e. the cell is modeled as a d-dimensional sphere with radius L. We assume that L takes the value 10 μm.
We eliminate the units of the magnitudes with the transformation $\bar{x} = x/L$ and $\bar{t} = t/\tau$, where the time scale $\tau = L^2/d_1$ is coupled to the diffusion rate d_1 and the length scale L. We divide the equations of the reaction-diffusion system, which consists of the reaction system (3) extended by the diffusion terms, by 100 nM, the order of the typical caspase concentration in KYM-1 cells. We get the reaction-diffusion system in the dimensionless form

$$\begin{array}{l} \frac{\partial X_a}{\partial \bar{t}} = \tilde{k}_{c1} X_i Y_a - \tilde{k}_{d1} X_a + D_1 \Delta_{\bar{x}} X_a, \\ \frac{\partial Y_a}{\partial \bar{t}} = \tilde{k}_{c2} Y_i X_a^n - \tilde{k}_{d2} Y_a + D_2 \Delta_{\bar{x}} Y_a, \\ \frac{\partial X_i}{\partial \bar{t}} = -\tilde{k}_{c1} X_i Y_a - \tilde{k}_{d3} X_i + \tilde{k}_{p1} + D_3 \Delta_{\bar{x}} X_i, \\ \frac{\partial Y_i}{\partial \bar{t}} = -\tilde{k}_{c2} Y_i X_a^n - \tilde{k}_{d4} Y_i + \tilde{k}_{p2} + D_4 \Delta_{\bar{x}} Y_i, \end{array} \tag{5}$$

in $\bar{\Omega} := \{\bar{x} \in \mathbb{R}^d, \|\bar{x}\| \leq 1\}$ with $D_1 = 1, D_2 = d_2/d_1, D_3 = d_3/d_1, D_4 = d_4/d_1$. The values for the diffusion coefficients $d_1, \ldots, d_4$ can be found for instance in [3, 11, 12], namely

$$d_1 = 18 \ \frac{\mu\text{m}^2}{\text{s}}, d_2 = 18.6 \ \frac{\mu\text{m}^2}{\text{s}}, d_3 = 18.9 \ \frac{\mu\text{m}^2}{\text{s}}, d_4 = 22.7 \ \frac{\mu\text{m}^2}{\text{s}}. \tag{6}$$

Hence, the ratios of the diffusion coefficients are $D_2 \approx 1.03$, $D_3 = 1.05$ and $D_4 \approx 1.26$.
Moreover, the reaction, production and degradation rates in the dimensionless form are

$$\begin{array}{ll} \tilde{k}_{c1} = k_{c1} \cdot \tau \cdot 100\,\text{nM} = 0.444, & \tilde{k}_{c2} = k_{c2} \cdot \tau \cdot (100\,\text{nM})^n = 0.444, \\ \tilde{k}_{dj} = k_{dj} \cdot \tau/60 = 0.0028, & \tilde{k}_{pi} = k_{pi} \cdot \tau/100\,\text{nM} = 5.556 \cdot 10^{-4}, \end{array} \tag{7}$$

$i = 1, 2; j = 1, \ldots, 4$. The reaction-diffusion system (5) has to be completed with boundary conditions. Instead of mixed boundary conditions describing the activation of pro-caspase 8 by death receptors at the cell membrane, we assume that there is no flux of caspases through the cell membrane, but assume simultaneously that a region near the boundary is initially filled with the death state $X^{(d)}$, whereas the rest of the cell is initially filled with the life state $X^{(l)}$. This assumption corresponds to a fast activation of pro-caspase 8 and pro-caspase 3 at the cell membrane by death receptors and active caspase 8, respectively. Physiologically, this resembles a situation where death receptors are activated by a pulse stimulus and subsequently deactivated, for example by receptor internalization and turnover. The death state $X^{(d)} := (X_a^{(d)}, Y_a^{(d)}, X_i^{(d)}, Y_i^{(d)})$ and the life state $X^{(l)} := (X_a^{(l)}, Y_a^{(l)}, X_i^{(l)}, Y_i^{(l)})$ will be computed in Section 3.

In detail our assumptions are as follows. System (5) is completed with homogeneous Neumann boundary conditions at the boundary $\partial\bar{\Omega}$ due to the assumption that there is no flux of caspases through the cell membrane. Moreover, we choose localized caspase concentrations as initial conditions

$$(X_a, Y_a, X_i, Y_i)(\bar{x}, 0) = \begin{cases} (X_a^{(d)}, Y_a^{(d)}, X_i^{(d)}, Y_i^{(d)}) \text{ for } \bar{x} \in \bar{\Omega}_{\text{ext}}, \\ (X_a^{(l)}, Y_a^{(l)}, X_i^{(l)}, Y_i^{(l)}) \quad \text{for } \bar{x} \in \bar{\Omega}_{\text{in}} \end{cases} \tag{8}$$

with

$$\bar{\Omega}_{\text{ext}} := \{\bar{x} \in \mathbb{R}^d, R_0 \leq \|\bar{x}\| \leq 1\} \text{ and } \bar{\Omega}_{\text{in}} := \{\bar{x} \in \mathbb{R}^d, \|\bar{x}\| < R_0\} \tag{9}$$

for an arbitrary but fixed $R_0 \in (0, 1)$. Finally, we introduce the short form of the reaction-diffusion system (5)

$$\frac{\partial u}{\partial \bar{t}} = D \Delta_{\bar{x}} u + f(u) \tag{10}$$

with $u = (X_a, Y_a, X_i, Y_i)^\top, D = \text{diag}\{1, D_2, D_3, D_4\}$ and the function $f(u)$ containing the reaction kinetics of (5). Equation (10) is more easy to handle in the stability analysis in Section 3.

Since we are interested in the question which of the two asymptotically stable steady states, namely the life state and the death state, is approached in the spatially extended model, we first compute in Section 3 the two stable steady states denoted with $X^{(d)}$ and $X^{(l)}$. Afterward, we study the stability of these steady states.

3 The steady states and their stability

The life state and the death state from [6] are time and space independent solutions $X = (X_a, Y_a, X_i, Y_i)$ of the reaction-diffusion system (5) and satisfy the equations

$$\begin{aligned} \tilde{k}_{c1} X_i Y_a - \tilde{k}_{d1} X_a &= 0, \\ \tilde{k}_{c2} Y_i X_a^n - \tilde{k}_{d2} Y_a &= 0, \\ -\tilde{k}_{c1} X_i Y_a - \tilde{k}_{d3} X_i + \tilde{k}_{p1} &= 0, \\ -\tilde{k}_{c2} Y_i X_a^n - \tilde{k}_{d4} Y_i + \tilde{k}_{p2} &= 0. \end{aligned} \tag{11}$$

By expressing Y_a, X_i and Y_i subject to X_a we get one nonlinear equation for X_a

$$\begin{aligned} (\tilde{k}_{c1}\tilde{k}_{c2}\tilde{k}_{d1}\tilde{k}_{p2} + \tilde{k}_{c2}\tilde{k}_{d1}\tilde{k}_{d2}\tilde{k}_{d3}) X_a^{n+1} - \tilde{k}_{c1}\tilde{k}_{c2}\tilde{k}_{p1}\tilde{k}_{p2} X_a^n \\ + \tilde{k}_{d1}\tilde{k}_{d2}\tilde{k}_{d3}\tilde{k}_{d4} X_a = 0. \end{aligned} \tag{12}$$

The first solution denoted with $X^{(l)} := (X_a^{(l)}, Y_a^{(l)}, X_i^{(l)}, Y_i^{(l)})$ is given by

$$X^{(l)} = (0, 0, \frac{\tilde{k}_{p1}}{\tilde{k}_{d3}}, \frac{\tilde{k}_{p2}}{\tilde{k}_{d4}}) = (0, 0, 0.2, 0.2).$$

This solution exists independently of the choice of the parameter values and the exponent $n \geq 1$ as long as $\tilde{k}_{d3} \neq 0 \neq \tilde{k}_{d4}$. For finding the other solutions we have to solve the equation

$$(\tilde{k}_{c1}\tilde{k}_{c2}\tilde{k}_{d1}\tilde{k}_{p2} + \tilde{k}_{c2}\tilde{k}_{d1}\tilde{k}_{d2}\tilde{k}_{d3}) X_a^n - \tilde{k}_{c1}\tilde{k}_{c2}\tilde{k}_{p1}\tilde{k}_{p2} X_a^{n-1} + \tilde{k}_{d1}\tilde{k}_{d2}\tilde{k}_{d3}\tilde{k}_{d4} = 0. \tag{13}$$

When there is no cooperativity, i.e. $n = 1$, then equation (12) has at most two real solutions and hence, the system exhibits no bistable behavior. In the following we study the case $n = 2$. We solve (13) numerically and receive two real-valued positive solutions

$$\begin{aligned} X^{(d)} &:= (X_a^{(d)}, Y_a^{(d)}, X_i^{(d)}, Y_i^{(d)}) = (0.1930, 0.1713, 0.0070, 0.0287), \\ X^{(u)} &:= (X_a^{(u)}, Y_a^{(u)}, X_i^{(u)}, Y_i^{(u)}) = (9.82 \cdot 10^{-4}, 3.08 \cdot 10^{-5}, 0.1990, 0.2000). \end{aligned}$$

In order to analyze the stability of these solutions we look at the Jacobian

$$J|_{X^*} = \begin{pmatrix} -\tilde{k}_{d1} & \tilde{k}_{c1} X_i & \tilde{k}_{c1} Y_a & 0 \\ 2\tilde{k}_{c2} Y_i X_a & -\tilde{k}_{d2} & 0 & \tilde{k}_{c2} X_a^2 \\ 0 & -\tilde{k}_{c1} X_i & -\tilde{k}_{c1} Y_a - \tilde{k}_{d3} & 0 \\ -2\tilde{k}_{c2} Y_i X_a & 0 & 0 & -\tilde{k}_{c2} X_a^2 - \tilde{k}_{d4} \end{pmatrix} \Bigg|_{X^*} \tag{14}$$

of the right hand side of the reaction system (3) evaluated at the steady states $X^* \in \{X^{(l)}, X^{(d)}, X^{(u)}\}$. The eigenvalues of the Jacobian for the three steady states are given by

$$\begin{aligned} X^{(l)} &: \lambda_{1,2,3,4}^{(l)} = -0.0028, \\ X^{(u)} &: \lambda_1^{(u)} = \lambda_2^{(u)} = -0.0028, \lambda_3^{(u)} \approx 0.0011, \lambda_4^{(u)} \approx -0.0067, \\ X^{(d)} &: \lambda_1^{(d)} = \lambda_2^{(d)} = -0.0028, \lambda_3^{(d)} \approx -0.0191, \lambda_4^{(d)} \approx -0.0791. \end{aligned} \tag{15}$$

We see that $X^{(l)}$ and $X^{(d)}$ are asymptotically stable and $X^{(u)}$ is unstable in the reaction system (3). Therefore, we get a bistable behavior for this special choice of parameter values.
In order to analyze the stability of the steady states $X^{(l)}, X^{(u)}$, and $X^{(d)}$ in the reaction-diffusion system (5), we consider (10) and follow the argumentation of Casten and Holland in [2]. Thus, we study the linearized system and conclude the local stability properties of the nonlinear system from the stability properties of the linearized system. We linearize the reaction-diffusion system (10) with respect to the stationary solution $X^* \in \{X^{(l)}, X^{(d)}, X^{(u)}\}$ by introducing the perturbation $z(\bar{x}, \bar{t})$, i.e. $u(\bar{x}, \bar{t}) = X^* + z(\bar{x}, \bar{t})$. This ansatz yields the linearized system for the perturbation of the stationary solutions

$$\frac{\partial z}{\partial \bar{t}} = D\Delta_{\bar{x}} z + J|_{X^*} z. \tag{16}$$

The stability of the zero solutions of the linearized system is determined by the eigenvalues $\mu_1(\lambda_k), \ldots, \mu_4(\lambda_k)$ of the matrix $M(\lambda_k) := J|_{X^*} - \lambda_k D$, where λ_k, $k = 0, 1, 2, \ldots$, are the eigenvalues to the eigenfunctions $\varphi_k \in \mathbb{R}^1$ of the Laplace operator, i.e. they fulfill the equation

$$-\Delta\varphi_k = \lambda_k \varphi_k \text{ in } \Omega = \{x \in \mathbb{R}^d | \, \|x\| \leq 1\} \tag{17}$$

with homogeneous Neumann boundary conditions $\frac{\partial \varphi_k}{\partial n}|_{\partial\Omega} = 0$, cf. Theorem 1 in [2]. For simplicity, we restrict the eigenvalue problem to the one-dimensional case, i.e. $\Omega = [-1, 1]$, and the Laplace operator is replaced by the second derivative. Hence, the eigenvalue problem becomes

$$-\varphi_k'' = \lambda_k \varphi_k \text{ in } [-1, 1] \tag{18}$$

with homogeneous Neumann boundary conditions $\varphi_k'(-1) = \varphi_k'(1) = 0$. The eigenvalues are $\lambda_k = \pi^2 \cdot k^2$ and the corresponding standardized eigenfunctions are $\varphi_k(x) = \frac{\sqrt{2}}{2} \cos(k\pi x), k \in \mathbb{N}_0$.

With the eigenvalues $\lambda_k, k \in \mathbb{N}_0$, at hand we compute the eigenvalues of the matrix $M(\lambda_k)$ for the three steady states.

i) For $X^* = X^{(l)}$ the real part of each eigenvalue $\mu_1(\lambda_k), \ldots, \mu_4(\lambda_k)$ of the matrix $M(\lambda_k)$ takes negative values for all eigenvalues $\lambda_k, k = 0, 1, \ldots$, and the maxima of the eigenvalues of $M(\lambda_k)$ are reached for λ_0, see Fig. 1,

$$\max_{k \in \mathbb{N}_0}(\mathrm{Re}(\mu_i^{(l)}(\lambda_k))) \approx -0.0028, i = 1, \ldots, 4.$$

Hence, the zero solution is asymptotically stable for the linearized system (16) and Theorem 2 in [2] yields the asymptotic stability of $X^{(l)}$ for the reaction-diffusion system (10).

ii) For the steady state $X^* = X^{(u)}$, the real part of one eigenvalue takes a positive value for λ_0. The maxima of the real part of the eigenvalues $\mu_1(\lambda_k), \ldots, \mu_4(\lambda_k)$ are

$$\begin{aligned}
&\max_{k \in \mathbb{N}_0}(\mathrm{Re}(\mu_1^{(u)}(\lambda_k))) = \max_{k \in \mathbb{N}_0}(\mathrm{Re}(\mu_2^{(u)}(\lambda_k))) \approx -0.0028, \\
&\max_{k \in \mathbb{N}_0}(\mathrm{Re}(\mu_3^{(u)}(\lambda_k))) \approx 0.0011, \max_{k \in \mathbb{N}_0}(\mathrm{Re}(\mu_4^{(u)}(\lambda_k))) \approx -0.0067.
\end{aligned}$$

Hence, the zero solution is unstable for the linearized system (16) and thereby the stationary solution $X^{(u)}$ is unstable for the system (10).

iii) For $X^* = X^{(d)}$ the real part of each eigenvalue $\mu_1(\lambda_k), \ldots, \mu_4(\lambda_k)$ is negative, cf. Fig. 1, and the maxima are reached for λ_0

$$\begin{aligned}
&\max_{k \in \mathbb{N}_0}(\mathrm{Re}(\mu_1^{(d)}(\lambda_k))) = \max_{k \in \mathbb{N}_0}(\mathrm{Re}(\mu_2^{(d)}(\lambda_k))) \approx -0.0028, \\
&\max_{k \in \mathbb{N}_0}(\mathrm{Re}(\mu_3^{(d)}(\lambda_k))) \approx -0.0191, \max_{k \in \mathbb{N}_0}(\mathrm{Re}(\mu_4^{(d)}(\lambda_k))) \approx -0.0791.
\end{aligned}$$

Hence, the zero solution is asymptotically stable for the linearized system (16) and the stability of $X^{(d)}$ for the reaction-diffusion system (10) follows from Theorem 2 in [2].

Remark 1 In [6] bistable behavior of the system (3) has been shown with the help of the phase portrait for a reduced system in the case $n = 2.5$. In general, system (3) shows bistable behavior for all values $n > 1$, corresponding to cooperativity in caspase activation, and a certain choice of parameter values, cf. (12).

The analysis here is only for the case where bistability is generated from cooperativity in caspase activation. According to the results in [6], similar results are expected for model variants where bistability is either due to binding of caspase 3 to an inhibitor or zero-order ultrasensitivity in caspase degradation.

In Section 3, we showed that the reaction-diffusion system (5) possesses two spatially homogeneous, asymptotically stable steady states and one spatially homogeneous, unstable steady state. In Section 4, we investigate which of the two asymptotically stable steady states is approached for a given initial condition of the reaction-diffusion system.

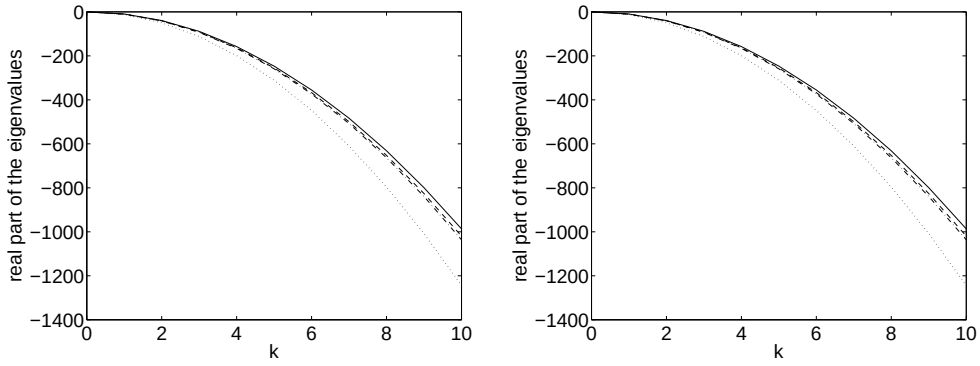

Fig. 1 Eigenvalues of the matrix $M(\lambda_k)$ for $X^{(l)}$ (left panel) and for $X^{(d)}$ (right panel) dependent on the mode k. For $X^{(l)}$ and $X^{(d)}$ the eigenvalues of the matrix $M(\lambda_k)$ are negative for all $k \in \mathbb{N}_0$.

4 Analysis of spatial inhibition effects

With the steady states at hand we come back to the initial value problem stated in Section 2. For the numerical simulations, we simplify the model and restrict ourselves to radially symmetric caspase concentrations. So, the $(d+1)$- dimensional reaction-diffusion system (5) with d space dimensions and one time dimension is reduced to an effective two-dimensional model with one spatial dimensionless coordinate r and one time coordinate $\bar{t}$. The Laplace operator $\Delta_{\bar{x}}$ for radially symmetric functions is given by

$$\Delta_{\bar{x}} w = \frac{1}{r^{d-1}} \frac{\partial}{\partial r} \left(r^{d-1} \frac{\partial w}{\partial r} \right), \; w \in \{X_a, Y_a, X_i, Y_i\}, d = 1, 2, 3. \tag{19}$$

Under these assumptions, the reaction-diffusion system (5) becomes

$$\begin{aligned}
\tfrac{\partial X_a}{\partial \bar{t}} &= \tilde{k}_{c1} X_i Y_a - \tilde{k}_{d1} X_a + \tfrac{1}{r^{d-1}} \tfrac{\partial}{\partial r} (r^{d-1} \tfrac{\partial X_a}{\partial r}), \\
\tfrac{\partial Y_a}{\partial \bar{t}} &= \tilde{k}_{c2} Y_i X_a^n - \tilde{k}_{d2} Y_a + D_2 \tfrac{1}{r^{d-1}} \tfrac{\partial}{\partial r} (r^{d-1} \tfrac{\partial Y_a}{\partial r}), \\
\tfrac{\partial X_i}{\partial \bar{t}} &= -\tilde{k}_{c1} X_i Y_a - \tilde{k}_{d3} X_i + \tilde{k}_{p1} + D_3 \tfrac{1}{r^{d-1}} \tfrac{\partial}{\partial r} (r^{d-1} \tfrac{\partial X_i}{\partial r}), \\
\tfrac{\partial Y_i}{\partial \bar{t}} &= -\tilde{k}_{c2} Y_i X_a^n - \tilde{k}_{d4} Y_i + \tilde{k}_{p2} + D_4 \tfrac{1}{r^{d-1}} \tfrac{\partial}{\partial r} (r^{d-1} \tfrac{\partial Y_i}{\partial r}).
\end{aligned} \tag{20}$$

The radially symmetric reaction-diffusion system (20) is completed with homogeneous Neumann boundary conditions at the boundaries $r = 0$ and $r = 1$; at the boundary $r = 0$ because of the smoothness of the radially symmetric concentration distribution at the center and at the boundary $r = 1$ due to the assumption that there is no flux of caspases through the cell membrane. Moreover, we consider localized caspase concentrations as initial conditions, cf. (8).

Hence, we study the competition between a spatially localized death state corresponding to high active caspase concentrations close to the cell membrane and the life state corresponding to low active caspase concentrations in the interior of the cell. If the region initially occupied by the death state is small the life state wins against the death state so that the complete cell is finally filled with the life state again. In order to establish this behavior we solve the reaction-diffusion system (20) with an implicit Euler scheme where the spatial derivatives are discretized with a first order centered finite difference method [10].

We observe the following behavior. The dynamics can roughly be separated in two steps. At the beginning the diffusion process is much faster than the reaction kinetics. After about 3 seconds the diffusion process has balanced the gradient in the caspase concentrations and yields an almost homogeneous distribution of caspase molecules, see Fig. 2 and Fig. 3. Afterward, the diffusion process is almost irrelevant for the dynamics and the reaction kinetics determines the behavior of the system. Thus, we solve the reaction-diffusion system (20) with homogeneous Neumann boundary conditions until the gradient in the concentrations is smoothed by the diffusion process and solve subsequently the ODE system corresponding to the reaction kinetics with the values of the almost homogeneously distributed caspase concentrations as initial conditions.

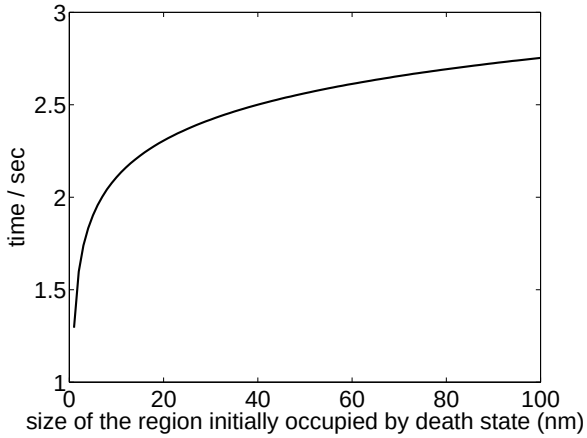

Fig. 2 The time passed until the gradient in the caspase concentrations is smoothed by the diffusion process depends on the size of the region initially occupied by the death state.

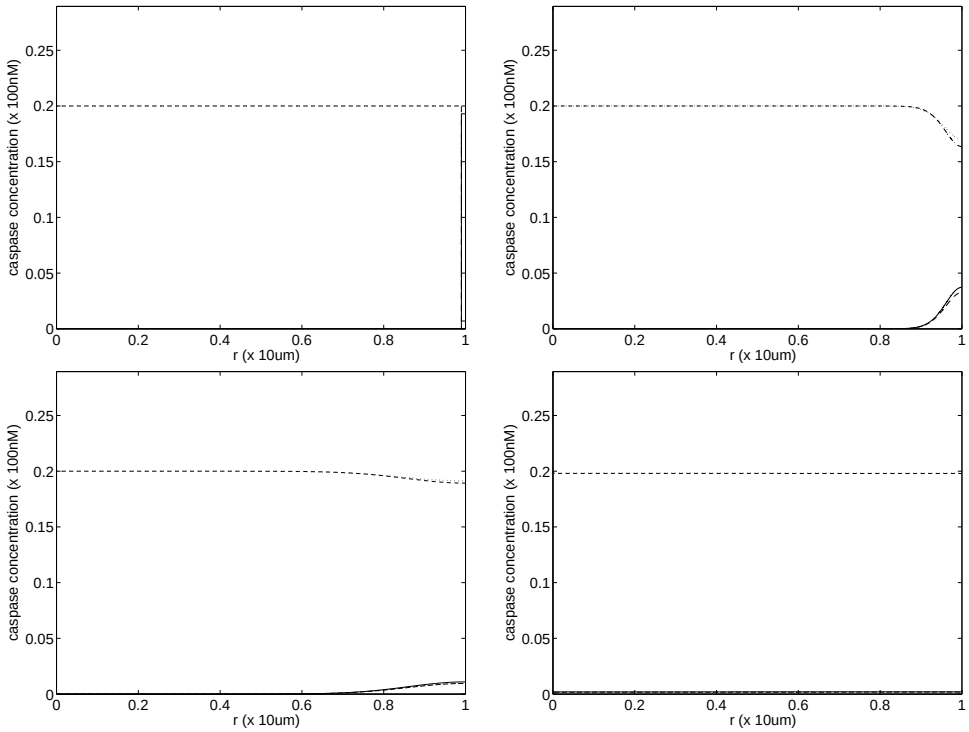

Fig. 3 Numerical solution of the radially symmetric reaction-diffusion system (20) with homogeneous Neumann boundary conditions after 1 (left top), 10 (right top), 100 (left bottom) and 5000 (right bottom) time-steps in the case $d = 1$. The step-size in time is $\Delta t = 1/10000$, multiplied with $\tau = 50/9$ s yields a "homogenization time" of about 2.5 s. The mesh size for the spatial discretization is $\Delta r = 0.0001$ and $R_0 = 0.99$.

The simulation is stopped at the time $t = t^*$ if $\mathrm{dist}^{(l)}(t^*) < 10^{-1}$ or $\mathrm{dist}^{(d)}(t^*) < 10^{-1}$ where $\mathrm{dist}^{(*)}(t) := \max_{v\in\{X_a,Y_a,X_i,Y_i\}}\{|v(t) - v^*|/|v^{(u)} - v^*|\}$ and the star is replaced either by 'd' for the death state or 'l' for the life state. The stopping criterion $\mathrm{dist}^{(l)}(t^l) < 10^{-1}$ defines the "life time" t^l and the criterion $\mathrm{dist}^{(d)}(t^d) < 10^{-1}$ the "death time" t^d. With this numerical simulation, we finally find the critical value $R_c = \sup\{R_0, \text{where } R_0 \text{ is the size of the region where the life state wins}\}$ for the initial condition of the reaction-diffusion system (20). The physical value for R_c is computed to be in one dimension $R_c^{1d} = 4\,\mathrm{nm}$, in two dimensions $R_c^{2d} = 2\,\mathrm{nm}$, and in three dimensions $R_c^{3d} = 1\,\mathrm{nm}$.

The spherical shell initially, homogeneously filled with caspase 3 and caspase 8 approximately has a volume of $1.26\,\mu\text{m}^3$. Since we consider a cell modeled by a sphere with radius $10\,\mu\text{m}$ and volume $V \approx 4.19 \cdot 10^3\,\mu\text{m}^3$, the death state initially occupies less than one per mill of the cell. For this size of death region, the death state does not succeed to invade the region occupied by the life state but for larger regions of initial caspase activation, the death state will ultimately cover the complete cellular volume. In addition to the value for R_c, we get with numerical simulations the dependence of the "death time" on the size of the region initially occupied by the death state, see Fig. 4. The time passed until the cell dies is of a realistic biological order, since in living cells or in manipulated cells produced for experiments, it takes about 15 minutes from stimulation of the signaling pathway to the occurrence of cell death. The simulations yield in the three-dimensional case for radially symmetric concentration distributions a death time of 30 to 250 minutes dependent on the strength of the initial activation, i.e. the size of the region initially filled with the death state.

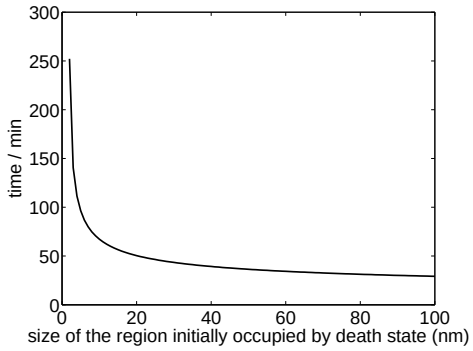

Fig. 4 The figure shows the dependence of the "death time" on the size of the region initially occupied by the death state in the three-dimensional case. Again, we choose $\Delta r = 0.0001$.

Similar results are obtained also for initial conditions different from the death state close to the boundary: taking arbitrary initial conditions where the caspase 8 and caspase 3 concentrations are high close to the boundary of the cell and where the rest of the cell is filled with the life state shows the same effects. Again diffusion will homogenize the caspase concentrations within a few seconds. Afterward the concentrations will be governed by the original reaction system. Concentrations of caspase 8 and caspase 3 above the ones of the death state will decrease the time which is necessary to kill the cell. Therefore, the important variable is the averaged initial concentration of caspase 8 and caspase 3, i.e. for a fixed cell the total number of caspase 8 and caspase 3 molecules at the beginning of the apoptosis process.

We see that the spatial extension of the cell leads to an inhibition effect of apoptosis. There is a threshold of area which has to be occupied by the death state before the death state can invade the region occupied by the life state.

5 Discussion

In this study, we introduced a spatial extension of the caspase cascade model established in [6]. Similar to [6] we computed the steady states of the reaction system and analyzed the stability properties. For our chosen parameter setting, we found two asymptotically stable and one unstable steady states. The values for the life state and the transition state are located close to each other, more precisely the difference in the concentrations is of the order pM. Nevertheless, the difference of the concentrations in a cell with radius 10 μm amounts to at least 8 molecules. The difference in the other components is much larger. Thus, the steady states are biologically distinguishable. Furthermore, the location of the steady states in the phase space depends on the choice of the parameter values and the difference between the steady state concentrations is larger for other choices of parameter values.
For the spatial extension of the model introduced in [6], we assumed for simplicity that the dynamics

of the caspase molecules in space obeys a diffusion process. We showed stability properties of spatially homogeneous stationary solutions and solved the reaction-diffusion system in the case of radially symmetric caspase concentrations numerically for several initial conditions and homogeneous Neumann boundary conditions. In [14], a radially symmetric reaction-diffusion system is used for modeling the MAPK pathway and phosphorylation waves traveling over long distances with constant amplitude and high velocity were found. In our case, the radially symmetric reaction-diffusion system (20) introduced in Section 4 does not allow the existence of traveling wave solutions on the biological scale of interest. We discuss the non trivial spatio-temporal structure of the numerical solution of (20) in the A.
In our model, we assumed that the activation of pro-caspase 8 by death receptors at the cell membrane occurs on a very small time scale in relation to the diffusion process, so that the activation of pro-caspase 8 by death receptors is integrated into the model as initial condition. Physiologically, this pulse stimulus corresponds to a death receptor internalization and turnover.
In order to analyze spatial inhibition effects, we studied the behavior of the system in dependence of the strength of the initial caspase activation with numerical simulations. The strength of the activation corresponds to the size of the region initially occupied by active caspase 3 and caspase 8. The simulation showed that the system possesses a switch-like behavior referred to the activation strength. For a spherical shell with a thickness of 1 nm, which is initially filled with the death state, the initial activation is not sufficient to transfer the signal to the nucleus and the cell is finally filled with the life state. For the KYM-1 cell, modeled by a sphere with radius 10 μm, the spherical shell with a thickness of 1 nm has a volume of 1.26 μm^3 and the initial concentration of activated caspases corresponds to 15 molecules. That means, 15 molecules of initially activated caspase 8 and caspase 3 homogeneously distributed at the cell membrane are not sufficient to kill the cell. But, if the spherical shell initially filled with active caspase has a thickness of 2 nm, the cell is finally filled with the death state. This initial concentration of caspase 3 and caspase 8 correspond to 30 molecules per caspase type. Thus, we find that the spatially extended model of caspase activation provides an apoptotic switch in the spatial dimension.

6 Conclusion

For a reaction-diffusion model for the description of the caspase cascade we showed the existence of two asymptotically stable and one unstable, spatially homogeneous stationary solution. Further investigations of the reaction-diffusion model indicate that the dynamics of the caspase concentrations happen in two steps. The first step is dominated by diffusion and takes only a few seconds. Heterogeneous initial conditions are homogenized in space by this process. In the second step there is pure ODE dynamics. Thus, after the homogenization process the original model of Eissing et al [6] is sufficient for the description of the apoptosis process. We showed with numerical simulations that the spatially extended model of caspase activation provides an apoptotic switch in the spatial dimension.
In order to confirm that spatial effects after the first diffusion step do not play any further role we compute in the appendix the relevant spatio-temporal structures in a spatially extended domain, namely the front solutions which describe the spreading of the death state into the region occupied by the life state. It turns out that these structures are by a factor 100 too large to fit into a cell.

A The size of the relevant spatial structures

A typical characteristic of bistable reaction-diffusion systems for $d = 1$ is the existence of traveling wave solutions connecting the two asymptotically stable steady states, cf. [9, Section 5]. In Section 4 we solved the reaction-diffusion system with homogeneous Neumann boundary conditions and certain initial conditions but the numerical solution did not show the structure of a traveling wave solution. In order to analyze the spatio-temporal structures of the solution, we solve the reaction-diffusion system with homogeneous Neumann boundary conditions and the initial conditions

$$X(r,0) = X^{(l)} \text{ for } 0 \le r < 500 \text{ and } X(r,0) = X^{(d)} \text{ for } 500 \le r \le 1000$$

on the interval $[0, 1000]$. Although for $d \ge 2$ no exact traveling wave solution exists, a similar behavior occurs. For the numerically observed front like solution the death state expands into the region occupied by the life state, cf. Fig. 5. There is one prescribed velocity $\bar{c}$ of the front which is independent of the chosen initial condition. Our numerical experiments show a front like behavior with an approximate velocity $|\bar{c}| \approx 0.2124$ for the chosen

parameter values in the case $d = 3$. Then, taking $L = 10$ μm, the physical wave speed is $|c_{\text{phys}}| \approx 0.382 \frac{\mu\text{m}}{\text{s}}$. This behavior is robust with respect to perturbations of the initial conditions and with respect to variations of the parameters. In order to study the robustness concerning variations in the parameter values we choose the parameter values $\tilde{k}_{c1} = \tilde{k}_{c2} = 0.444$, $\tilde{k}_{p1} = \tilde{k}_{p2} = 5.556 \cdot 10^{-4}$ and four pairwise different degradation rates $\tilde{k}_{d1} = 0.0028$, $\tilde{k}_{d2} = 0.0025$, $\tilde{k}_{d3} = 0.0022$ and $\tilde{k}_{d4} = 0.0033$. Here, the degradation rates are arbitrarily chosen. The structure of the solution is depicted in Fig. 5. The numerical simulation shows the existence of a front like

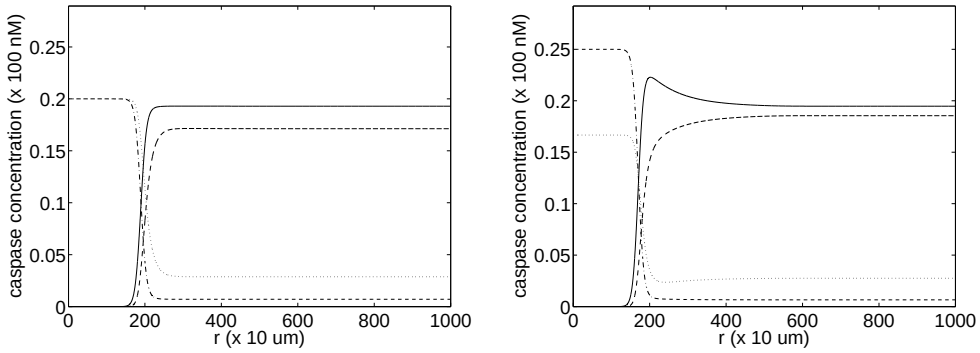

Fig. 5 Traveling wave solution which moves from the right to the left for $\tilde{k}_{d1} = \tilde{k}_{d2} = \tilde{k}_{d3} = \tilde{k}_{d4}$ (left panel) and non-monotone traveling wave solution which moves from the right to the left for pairwise different degradation rates (right panel) in the case $d = 3$ for the radially symmetric reaction-diffusion system (20). Solid line: caspase 8, dashed line: caspase 3, dash-dotted line: pro-caspase 8, dotted line: pro-caspase 3

solution connecting the two asymptotically stable steady states. We notice that the structure of the front like solution is by a factor 100 too large to fit into the cell. If diffusion is reduced by obstacles by a factor 10^4 the size of the front is below the dimension of the cell. However, the speed of the front then will be so small that execution of cell death would take an unphysiologically long time. Biologically, this hints to the possibility that cells may survive a spatially confined high activation of caspases, when caspases are immobilized or at least have a significantly reduced diffusion coefficient.

References

1. M. Bentele, I. Lavrik, M. Ulrich, S. Stösser, D. W. Heermann, H. Kalthoff, P. H. Krammer, and R. Eils. Mathematical modeling reveals threshold mechanism in CD95-induced apoptosis. *J Cell Biol*, 166(6):839–851, Sep 2004.
2. R.G. Casten and C.J. Holland. Stability properties of solutions to systems of reaction-diffusion equations. *SIAM Journal on Applied Mathematics*, 33(2):353–364, 1977.
3. G. M. Cohen. Caspases: the executioners of apoptosis. *Biochem. J.*, 326(1):1–16, 1997.
4. N. N. Danial and S. J. Korsmeyer. Cell death: critical control points. *Cell*, 116(2):205–219, Jan 2004.
5. T. Eissing, H. Conzelmann, E. D. Gilles, F. Allgöwer, E. Bullinger, and P. Scheurich. Bistability analyses of a caspase activation model for receptor-induced apoptosis. *J. Biol. Chem.*, 279(35):36892–97, August 2004.
6. T. Eissing, S. Waldherr, F. Allgöwer, P. Scheurich, and E. Bullinger. Steady state and (bi-)stability evaluation of simple protease signalling networks. *BioSystems*, 90:591–601, 2007.
7. M. Fussenegger, J. E. Bailey, and J. Varner. A mathematical model of caspase function in apoptosis. *Nat Biotechnol*, 18(7):768–774, Jul 2000.
8. M. O. Hengartner. The biochemistry of apoptosis. *Nature*, 407(6805):770–776, Oct 2000.
9. D. Henry. *Geometric Theory of Semilinear Parabolic Equations*, volume 840 of *Lecture Notes in Mathematics*. Springer, 1981.
10. D. Hoff. Stability and convergence of finite difference methods for systems of nonlinear reaction-diffusion equations. *SIAM Journal on Numerical Analysis*, 15(6):pp. 1161–1177, 1978.
11. H. J. Huber, M. A. Laussmann, J. H. M. Prehn, and M. Rehm. Diffusion is capable of translating anisotropic apoptosis initiation into a homogeneous execution of cell death. *BMC Syst Biol*, 4:9, 2010.
12. M. Kruidering and G. I. Evan. Caspase-8 in apoptosis: The beginning of "the end"?. *IUBMB Life*, 50(2):85 – 90, 2000.
13. M. Lamkanfi, N. Festjens, W. Declercq, V. T. Berghe, and P. Vandenabeele. Caspases in cell survival, proliferation and differentiation. *Cell Death and Differentiation*, 14(1):44–55, 2007.
14. N.I. Markevich, M.A. Tsyganov, J.B. Hoek, and B.N. Kholodenko. Long-range signaling by phosphoprotein waves arising from bistability in protein kinase cascades. *Molecular Systems Biology*, 2(1), 2006.

15. A. Meager, LE Sampson, M. Grell, and P. Scheurich. Development of resistance to tumour necrosis factor (tnf [alpha]) in kym-1 cells involves both tnf receptors. *Cytokine*, 5(6):556–563, 1993.
16. J. D. Murray. *Mathematical Biology I: An Introduction*. Springer, 2002.
17. M. Rehm, H. J. Huber, H. Dussmann, and J. H. M. Prehn. Systems analysis of effector caspase activation and its control by x-linked inhibitor of apoptosis protein. *EMBO J*, 25(18):4338–4349, Sep 2006.
18. M. Rehm, H. J. Huber, C. T. Hellwig, S. Anguissola, H. Dussmann, and J. H. M. Prehn. Dynamics of outer mitochondrial membrane permeabilization during apoptosis. *Cell Death Differ*, 16(4):613–623, Apr 2009.
19. S. J. Riedl and Y. Shi. Molecular mechanisms of caspase regulation during apoptosis. *Nature Reviews Molecular Cell Biology*, 5:897–907, 2004.
20. Y. Shi. Mechanisms of caspase activation and inhibition during apoptosis. *Molecular Cell*, 9:459–470, 2002.